The role of Directed Energy Deposition atmosphere mode on the microstructure and mechanical properties of 316L samples

The Role of Directed Energy Deposition Atmosphere Mode on the Microstructure and Mechanical Properties of 316L Samples

Alberta Aversa[1], Abdollah Saboori[1], Erica Librera[2], Michele de Chirico[2], Sara Biamino[1], Mariangela Lombardi[1], Paolo Fino[1]

[1]Department of Applied Science and Technology, Politecnico di Torino, Corso Duca degli Abruzzi 24, 10129 Torino, Italy

[2]Prima Industrie SpA, Via Trino Pianezza 36, 10093 Collegno To, Italy

Abstract

Laser-Directed Energy Deposition was used to produce AISI 316L stainless steel samples. The effect of the protective atmosphere on the microstructure and mechanical performance of AISI 316L deposited parts was investigated by building samples using a simple nitrogen shielding gas or using a nitrogen-filled build chamber. The effect of the different processing conditions on the microstructure was evaluated by X-ray analysis, optical and scanning electron microscopy. Only slight differences in the cellular dendrites morphology of samples built under different protective atmosphere conditions were observed. However, the presence of oxides was monitored too: the oxides composition and area fraction were analysed and compared by image analyses, and it was demonstrated that the protective atmosphere mainly affects the oxides dimensions. The effect of the oxides and nitrogen pick-up on the mechanical performance of the samples was evaluated by tensile tests. The results revealed that the nitrogen-filled build chamber allowed the achievement of slightly higher tensile strength and elongation with respect to the other processing conditions as a consequence of the reduced size of the oxide inclusions.

Keywords: Directed Energy Deposition; 316L; atmosphere; oxide; tensile properties

1. Introduction

AISI 316L stainless steel is largely used for applications that require a high corrosion resistance such as offshore petrochemical plants and orthopaedic implants [1,2]. Conventionally, to reduce the manufacturing cost of these components and facilitate the production process, two as-cast elements were welded together [3]. Nowadays, new technologies such as metal Additive Manufacturing (AM) are recognized as powerful alternatives to the conventional manufacturing ones for medium batch production of 316L components.

Laser-Powder Bed Fusion (L-PBF) and Laser-Directed Energy Deposition (L-DED) certainly are the most common laser-based metal AM production technologies [4]. During a L-DED process, a focused laser beam melts the material directly fed through the nozzles on the previous layer or substrate [5]. The material, which can be a powder or a wire, rapidly melts and solidifies creating the scan tracks. This process is found to be a promising method to be used in the production of the various metallic materials made of steel, titanium, nickel, and aluminium alloys [6–9].

Moreover, with respect to L-PBF, L-DED presents some advantages such as a high building rate, the possibility to repair metallic components, to produce functionally graded compositions and to build large parts [4]. The last advantage is mainly related to the possibility to create a protective atmosphere directly on the melt pool simply by an inert shielding gas. This technological advantage spares the usage of an inert gas chamber which generally restrains the dimensions of the parts, mainly because of cost and time issues.

Recently the L-DED processability, microstructure and properties of 316L have been deeply investigated in various works [7,10–13]. The main results are that, as a consequence of the rapid cooling and of the directional thermal gradient, the microstructure of L-DED 316L parts is mainly made of large columnar grains containing fine austenitic cells surrounded by retained δ–ferrite [10,11]. This peculiar microstructure is the reason for the interesting mechanical properties of L-DED parts, which are generally higher than those of the same alloy processed by conventional technologies [7,12]. However, recent studies showed that many factors and processing parameters can affect the mechanical properties of L-DED 316L parts [2,7,12,14]. Zhang et al. and Ma et al., for example, showed that the Yield Strength (YS) and Ultimate Tensile Strength (UTS) of L-DED 316L strongly depended on the laser power and the scan speed used during the building process [2,12]. This effect was attributed to the reduced solidification rate and thermal gradient of the parts obtained using high power or low scan speed. Yadollahi et al. observed that the YS, the UTS and especially the elongation (ε) of L-DED 316L parts were heavily affected by the inter-layer time interval [7]. The authors demonstrated indeed that a long time interval caused high solidification rates and thermal gradients and consequently fine microstructures characterised by high strength and low ductility values [7].

Ma et al. demonstrated that L-DED 316L samples built with optimised parameters were characterised by high strength values, but the elongation did not reach the desired level [15]. The low ductility values were mainly attributed by the authors to the processing atmosphere and in particular to the oxides content in the deposited samples [15]. Saboori et al. recently demonstrated that the powder quality also has a strong effect not only on the YS and UTS of L-DED 316L parts but also on the elongation [16]. This phenomenon was also attributed to a large number of oxides present in samples built with recycled powder. Eo et al. investigated the relation of the mechanical properties of L-DED 316L parts realized with several building parameters and highlighted the role of the oxygen content [17]. In their study, the YS was proportional to the oxide numerical density indicating that the oxides had a strengthening effect [17].

These studies showed that the melt pool oxidation plays a fundamental role in the quality of L-DED 316L parts. Therefore, recently, many authors studied the nature and the effects of the non-metallic inclusions in L-DED and generally in AM stainless steels samples. Song et al. demonstrated that the oxygen partial pressure had a strong effect on the chemical composition and the morphology of the oxides in L-PBF 316L samples [18]. Saeidi et al. showed that the very fine oxides (d= 50 nm) present in 316L samples processed by L-PBF are one of the reasons for the high mechanical properties of the alloy [19]. Lou et al., on the contrary, revealed that these inclusions have a detrimental effect on the toughness and stress corrosion cracking resistance of AM 316L parts [20]. It can be summarised that the oxide morphology and composition depends on various aspects such as the powder composition, the building atmosphere and the solidification conditions [17].

Because of these reasons, questions about the best protective atmosphere conditions for L-DED stainless steel parts have been raised. The present work focuses, therefore, on the effect of the use of a N_2 shielding gas or a N_2 filled build chamber on the microstructure and the mechanical properties of L-DED 316L samples.

2. Materials and methods

A commercial gas atomised 316L powder having a particles size in the range of 50-150 µm (d10=63.3 µm, d50=85.4 µm, d90=135.2 µm) was used for the production of L-DED samples. Scanning Electron Microscope (SEM) images of the fresh powder are reported in Figure 1 and show that the particles have an almost spherical morphology. Moreover, it is found that the starting powder includes some defects such as satellites (red arrows in Figure 1(a)) and inclusions (yellow arrows in Figure 1 (b)).

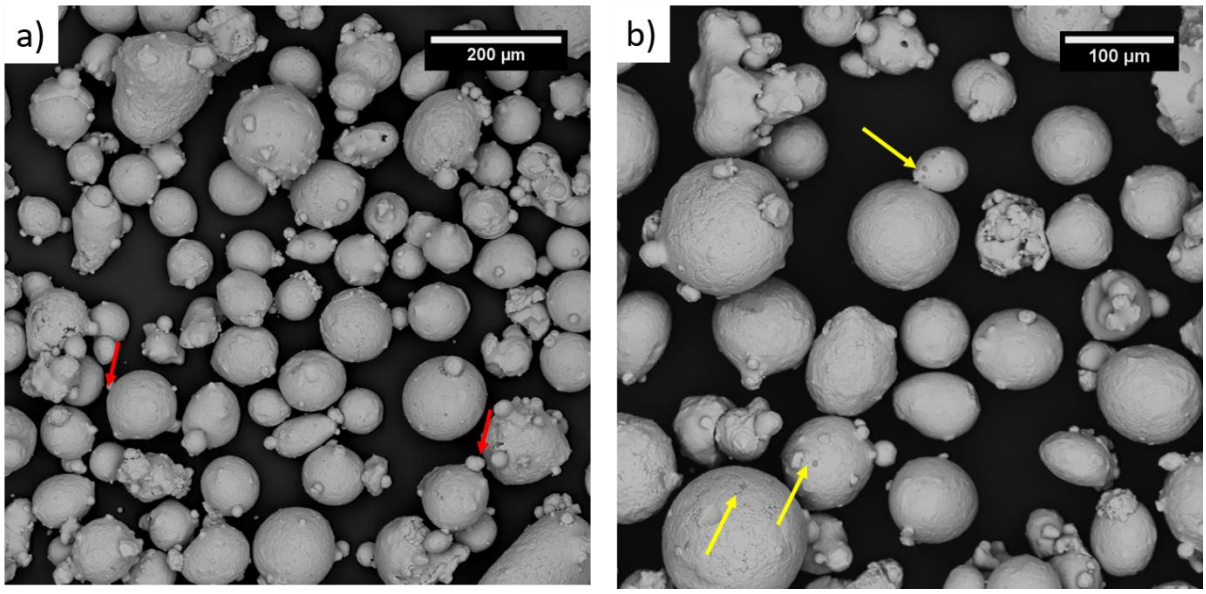

Figure 1 SEM images of 316L particles; red arrows show the satellites, yellow arrows indicate the inclusions.

The L-DED system used is a prototype produced by Prima Industrie S.p.A. composed by a 3-axis CNC unit described in our previous work [16]. The machine is equipped with an ytterbium laser with power up to 3 kW and four coaxial multi-nozzles. The powder was delivered by means of a commercial powder feeder using N_2 as a carrier gas. In order to study the effect of the atmosphere some samples were built using an N_2 shielding gas (SG) with a flow rate of 30 (L/min) while other samples were realized in an N_2-filled build chamber (BC). In the BC, other than the carrier gas, which brings the particles in the melt pool area, the only gas flow is located in the lateral part of the chamber and does not interact with the process. When the BC was used, the oxygen content was evaluated using a MultiExact 5400 – SERVOPRO sensor. The oxygen content was kept lower than 0.1 % during the whole building process. The oxygen sensor was not used during the SG building process as, in this case, the oxygen content varied within the process because of the movement of the deposition head. The samples were built on austenitic stainless steel plates having the following dimensions: 150 ×150 ×6 mm. Block (10 x10 x20 mm) and bar (93 x 12 x12 mm) samples (see Figure 2) were produced in both conditions: SG or BC. All samples were produced using the optimised parameters described in [21] that allow the obtainment of fully dense parts.

The block samples were cut along the building direction, polished down to 1 µm and etched for 2 s in a solution containing 15 ml HCl + 10 ml HNO_3 + 1 ml acetic acid. The microstructural analyses were carried out by a Leica DMI 5000 Optical Microscope (OM), a Phenom XL SEM and a Carl Zeiss MERLIN Field Emission Scanning Electron Microscope (FESEM) equipped with an Energy Dispersive X-ray Spectrometry (EDS) system. The inclusion content was investigated by means of the ImageJ software on the SEM images with a high magnification taken along the building direction (see locations indicated in Figure 2 a)). The area fraction at different distances from the substrate (at every 2.5 mm) was calculated on three images taken at the same height. The Primary Cellular Arm Spacing (PCAS) was evaluated by the triangle method on SEM images taken

at 5000 X. In the triangle method, three central points of any three adjacent cellular dendrites form a triangle. The average PCAS of the three cells is the average of three lengths of three sides of cellular dendrites. Each mean PCAS value is achieved by averaging 40 measurements at different distance from the substrate. At each specific distance from the substrate, three images were acquired from the left to right side (along the X direction) [2].

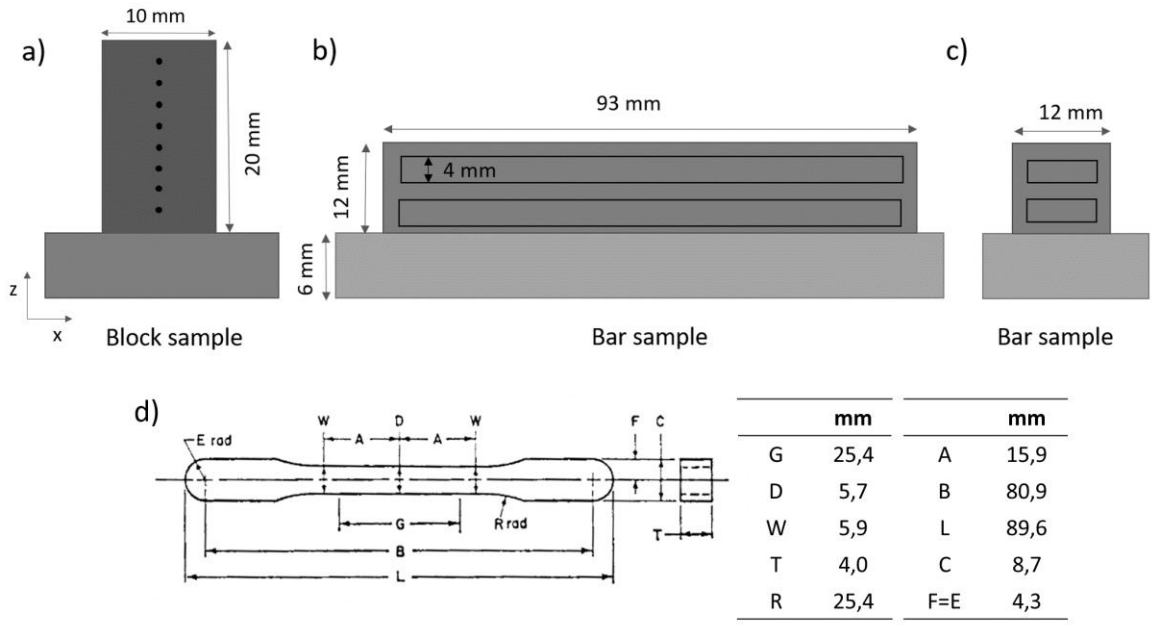

	mm		mm
G	25,4	A	15,9
D	5,7	B	80,9
W	5,9	L	89,6
T	4,0	C	8,7
R	25,4	F=E	4,3

Figure 2 Schematic representation of L-DED a) block samples (the dashed lines indicate the areas in which the SEM images were taken) and b), c) bar samples from which tensile samples were obtained.

The contaminations content, in terms of oxygen, nitrogen and hydrogen, of the powder and the dense samples were analysed using the inert gas fusion method by means of a LECO ONH836 Oxygen/Nitrogen/Hydrogen elemental analyser on three specimens extracted at different height from each block L-DED sample.

X-ray diffraction (XRD) analyses were carried out on the XZ cross-section of the block samples using an X-Pert Philips diffractometer (Cu Kα) in a Bragg Brentano configuration with 2θ range= 20-110° (operated at 40 kV and 40 mA with a step size 0.013 and 35 s per step).

Two tensile samples were machined from each 12 × 12 × 93 mm as-built bars (Figure 2 b) and c)). The tensile samples dimensions are based on the ASTM E-8 standard and had a 4 mm thickness (Figure 2 d)). The tensile samples were tested using a Zwick Z100 tensile machine using 8×10^{-3} s^{-1} as strain rate.

3. Results and discussion

3.1. Microstructure and composition

In general, in L-DED materials grains and dendrites, morphology and size are defined by the thermal history of the component. Previous studies demonstrated that, due to the rapid cooling and to the directional heat flow, L-DED 316L parts are characterised by large columnar grains containing γ-dendrites and δ-ferrite mainly located in the interdendritic zone [11].

The optical micrographs of the cross-sections of the 316L samples reported in Figure 3 confirm these results and show that the microstructures of SG and BC samples were similar and that, in both cases, large grains containing micrometric cells were formed during the L-DED process.

High magnification images (Figure 3c) and d)) reveal that the cells had various shapes and sizes depending on the location within the melt pool. Furthermore, dark spherical particles can be detected uniformly distributed in the cells and their boundaries in both images.

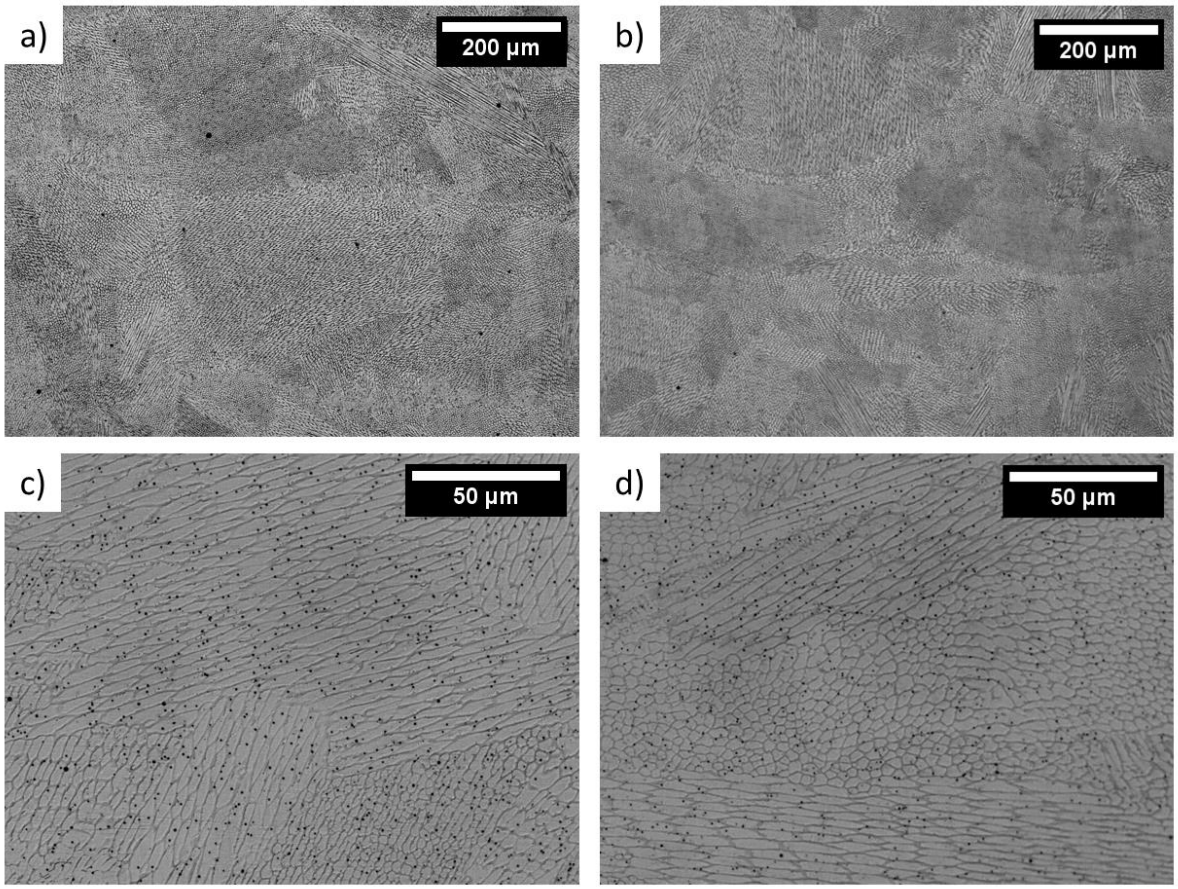

Figure 3 Optical micrographs of the cross-section of 316L L-DED samples built with (a, c) SG or (b, d) BC.

EDS analyses were carried out on these spherical particles in order to investigate their nature. The results reported in Figure 4 demonstrate that these non-metallic particles were rich in Si, Mn and O. In particular, EDS-line analyses highlighted that the larger particles contained Mn, Si and O while the finer ones contained only Si and O. The different size and chemistry indicate that during the building process oxides with different sizes were formed by specific mechanisms; the large and irregular oxides were generated due to the solidification of the slag layer, while the fine and spherical ones formed, upon the solidification, due to the low O solubility in steel [18]. The large oxide composition, detected by EDS, suggested that these are Rhodonite ($MnSiO_3$) which is a metastable phase that, due to the rapid cooling, is generally found in 316L AM samples [22]. The small oxide composition indicate that these are SiO_2 which was also detected only in a few works [17,23].

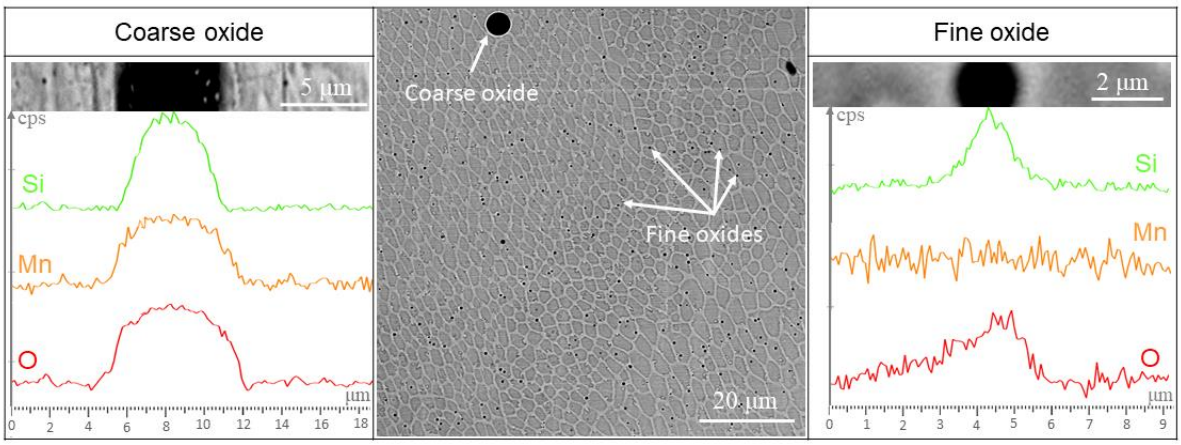

Figure 4 EDS-maps of a 316L sample built using SG.

The oxide area fraction results, reported in Figure 5, indicate the BC was more effective than the SG in preventing the oxidation of the material. In the BC case, in fact, samples have a lower oxide content than the SG ones along the whole sample height. As previously described, during the BC L-DED process, the oxygen concentration in the building atmosphere was monitored and kept below 0.1 %. In the SG case, on the contrary, the oxygen concentration might vary during the process due the movement of the deposition head. This different oxygen concentration might cause the different oxidation of the melt pool.

It is interesting to underline, however, that in both cases, oxidation took place and that the oxide area fraction slightly increased with the sample height. This trend might be correlated to the cooling rate trend within L-DED samples. The lower cooling rate of the higher part of the samples can explain the stronger tendency of the melt pool to absorb oxygen. Despite of having different and more complex trends along the Z direction in both cases, an overall increasing trend can be revealed.

The comparison of the SEM images of the upper part of the samples shows that the SG sample contained slightly larger oxides. The mean value of the oxide diameter resulted equal to 0.35±0.06 µm and 0.26±0.05 µm for the samples built with SG or BC, respectively.

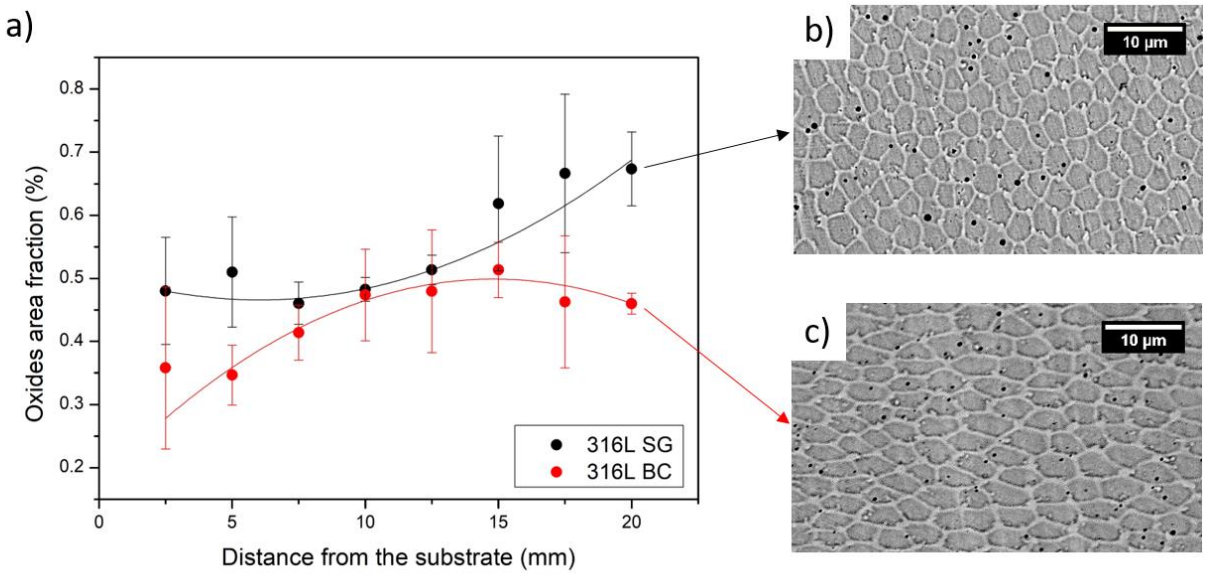

Figure 5 a) Oxide area fraction as a function of sample height of 316L samples built with SG or BC and SEM micrographs of the upper part of samples built b) with SG or c) with BC.

The LECO data of bulk samples are compared in Table 1 with the fresh powder ones. The results demonstrate that both processing conditions (SG and BC) cause a nitrogen pick-up during the process. In particular, the nitrogen content of BC samples was slightly higher than that of the SG ones but it is within the standard values (1000 ppm) according to ASTM A240/A240M. The increase in nitrogen content is most probably due to the usage of N_2 as protective gas during the L-DED process. Several studies also demonstrated that nitrogen is an important alloying element for stainless steel as it has several beneficial effects on its properties. Nitrogen can indeed increase the yield strength, the toughness the corrosion and the creep resistance of steels [24,25]. Because of this reason, using a nitrogen atmosphere during AM process, might be considered an easy method to slightly increase the N content of 316L parts.

The comparison of the oxygen content shows that the BC is more effective in avoiding the oxygen pick-up during the building process. The SG sample has in fact twice as much the oxygen content with respect to the powder and the BC sample. It must be pointed out that a stronger difference in the oxygen/oxide content was detected by LECO than by image analyses, this might be due to the presence of extremely fine oxides hardly detectable by SEM. A close look to the oxygen content of the powder and BC sample shows that this bulk sample has an even lower O content than the powder itself. This is probably due to the particles surface oxides that are considered in the results [14]. Based on the literature, the particles' surface oxides generate the melt pool surface oxide (slag layer) and, as the AM process proceeds, part of this oxide melts and float on top of the subsequent melt pools [17].

Finally, no hydrogen pick-up was found in the sample after the deposition in both conditions.

Table 1 LECO results of 316L powder and bulk samples produced with SG or BC

	N (ppm)	O (ppm)	H (ppm)
316L powder	9±23	354±2	6±1
316L-SG	849±27	642±11	3±1
316L-BC	945±28	346±1	4±0.5

Even if these results suggest that the BC was more effective in protecting the part from oxidation, both oxide content values are generally acceptable as part of the oxygen content comes from the powder itself.

Afterwards, the effect of protection mean, SG or BC, on the crystalline phase composition of 316L samples was evaluated by means of XRD analysis. Figure 6 reports the diffraction patterns of the starting 316L gas atomised powder and bulk samples built with SG or BC. The graph confirms that, in all cases, the microstructures consist mainly of austenite. Some differences related to the relative peaks intensity of powder and massive samples can be found. This diversity is due to the strong texture of L-DED samples caused by the substantial directional thermal gradient to which they are exposed during the production process [26]. Exploring in more detail the (200) peak (Figure 6b)), a slightly stronger texture can be observed in the BC sample pattern probably due to the different thermal conditions of these samples with respect to the SG ones [27]. As schematically represented in Figure 7, in fact, SG samples were surrounded by cold shielding gas while the BC samples by a more static hot atmosphere. Because of this reason, the BC samples had a more directional thermal gradient and therefore a stronger texture.

Previous studies on AM 316L samples revealed the presence of the high-temperature δ-ferrite phase with a peak at $2\theta = 44.3°$ [10,28]. In the present study, a slight hump right to the 42.9 ° peak was revealed in patterns

of both L-DED 316L samples. This might indicate a modest presence of the δ ferrite phase in both SG and BC samples that can be expected owing to a very high cooling rate during the L-DED process [28]. As a matter of fact, according to the Schaeffler predictive phase diagram, during the rapid solidification, the microstructure of austenitic stainless steel consists of austenite and δ-ferrite [29]. Nonetheless, it is interesting to underline that, depending on the proportion of Cr_{eq}/Ni_{eq}, different δ-ferrite morphologies, such as eutectic, skeletal, acicular and lathy, can be obtained [29]. In the present study, for the gas atomised powder Cr_{eq}/Ni_{eq}=1.69 locates the composition in the FA (Ferrite-Austenite) region in the Pseudo-binary phase diagram, therefore skeletal or lathy ferrite should solidify depending on the cooling rate. With this solidification mode, at high cooling rates the solidifying ferrite consumes δ-stabilizers such as Cr, Mo, and Si and consequently, the residual liquid fractions are rich in austenite promoting elements, therefore leading to the possibility to form austenite [29]. Due to the L-DED rapid cooling, the high temperature δ-ferrite can be retained at room temperature in as-built samples.

It is however also important to underline that nitrogen is a strong austenite stabiliser and that the Cr_{eq}/Ni_{eq} might shift due to the N pick-up (Table 1). The Cr_{eq}/Ni_{eq} of the samples calculated with the N content is 1.38. The N-pick up moves the composition from the 10 % to the 5 % ferrite and from the FA to the AF region of the Pseudo-binary phase diagram [25].

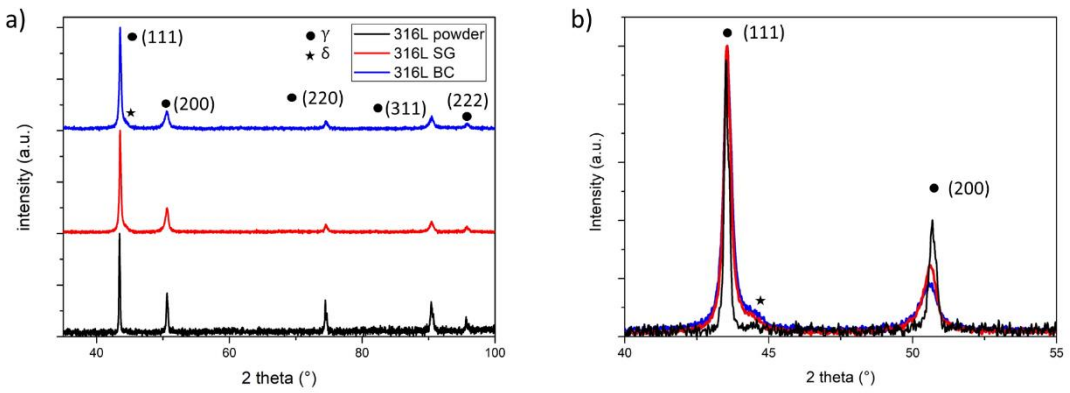

Figure 6 a) XRD pattern of L-DED 316L powder, SG sample and BC sample and b) inset of a) between 40 and 55 °.

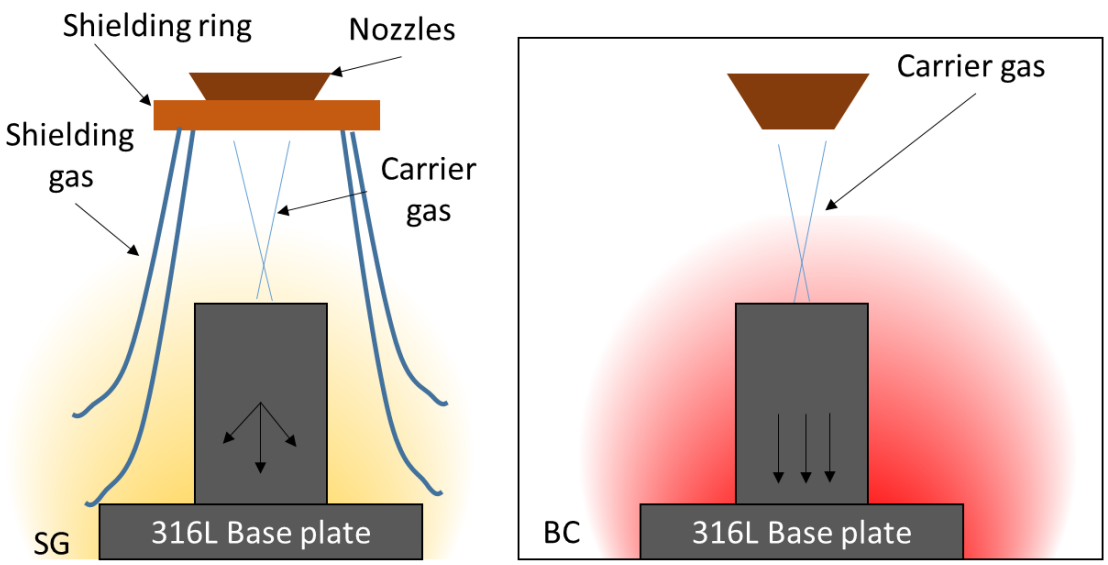

Figure 7 Schematic representation of the cooling condition of SG and BC samples.

The presence of the δ-ferrite was confirmed by FESEM micrographs of 316L samples cross-sections (Figure 8). The δ-ferrite of both samples is characterised by a skeletal morphology indicating an AF solidification mode from the liquid phase (L) that consists in [30]:

$$L \rightarrow L + \gamma \rightarrow L + \gamma + \delta \rightarrow \gamma + \delta$$

The FESEM images show also that the samples were characterised by very similar microstructures, however differences are hard to evaluate on single images due to fluctuation of cells size and morphology within the melt pool. Therefore, in order to clearly assess the differences in terms of cells size in the SG and BC samples, the PCAS values of the block samples at different height were evaluated by using the triangle method. In this method, proposed by Ma et al., a triangle is sketched so that its points are in the centre of three adjacent cells and the average PCAS is calculated as the average of the lengths of three sides the triangle [31].

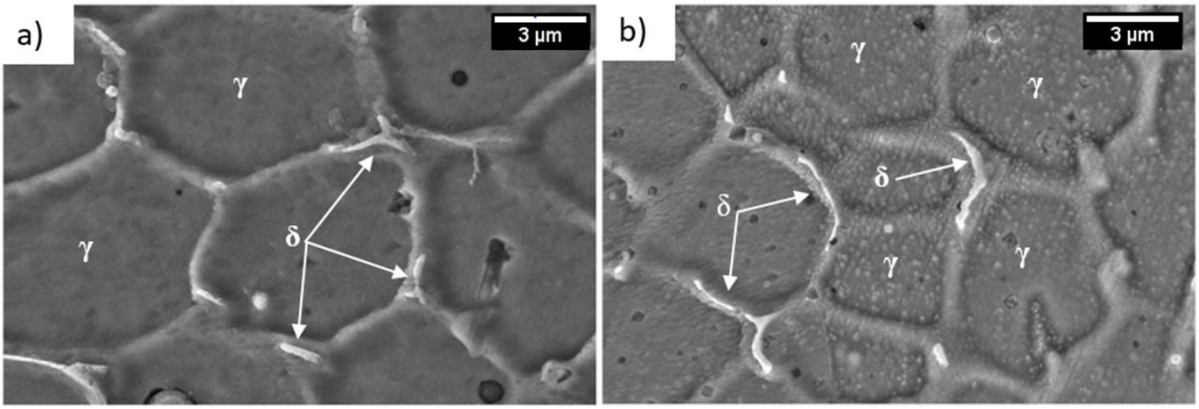

Figure 8 FESEM micrographs of L-DED 316L samples cross sections built with a) SG or b) BC.

The PCAS trend of the 316L SG and BC samples is reported in Figure 9 and, in both samples, it varied in the range between 2.8 µm and 4.5 µm and increased with the sample height. This trend was observed in previous

studies and is attributed to the different cooling rates in different distance from the substrate [16]. It is also interesting to underline that the last layer did not follow this ascending trend as it was characterised by a lower PCAS with respect to the previous one. This effect could be due to the lack of intrinsic heat treatment of the last layer [32]. Similar PCAS trends and values were observed in the samples built using SG and BC, confirming that the atmosphere did not affect the cooling rate and, accordingly, PCAS. It is worth to underline that the PCAS trend is similar to the oxides one (Figure 5) suggesting that the oxide size might be correlated to the cooling rate.

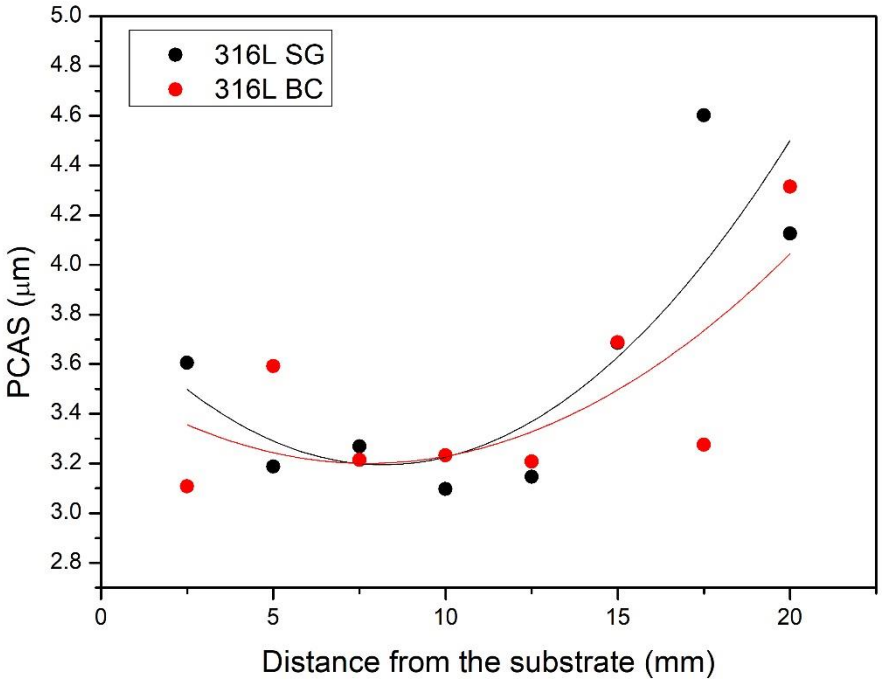

Figure 9 PCAS as a function of the distance from the substrate for the sample built with SG or BC.

3.2. Mechanical Properties

Two representative tensile curves of 316L samples built using SG or BC are reported in Figure 10. The curves show that the sample built in the build chamber is characterised by slightly higher mechanical properties than that realized with the shielding gas. In particular, higher *YS*, *UTS* and ε were achieved thanks to the protective atmosphere of the build chamber.

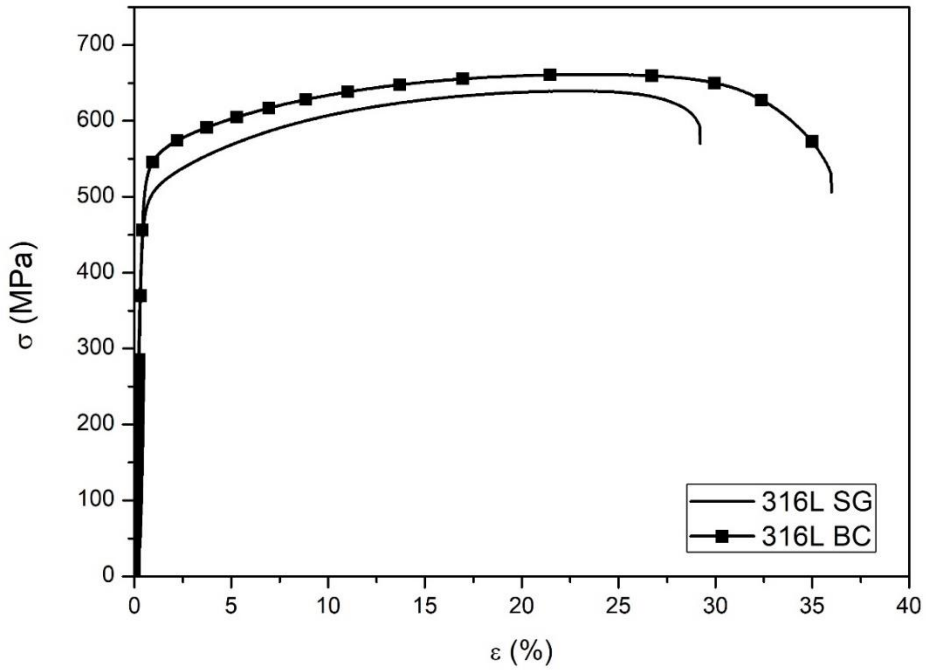

Figure 10 Representatives tensile curves of L-DED 316L samples built with SG and in BC

The mechanical properties of L-DED 316L samples, compared in Table 2, indicate that the build chamber allowed a 12% increase in the YS with respect to the SG condition. A slight increase in UTS and ε was also observed.

As the main difference among SG and BC samples microstructure is to be found in the oxide content and size, the variation in the mechanical properties can be probably found in these inclusions strengthening phenomena [33]. As a matter of fact, both, oxide quantity and size, affect the Orowan strengthening which can be calculated based on the stress required to the dislocation to bow between inclusions. The shear value depends on the dislocation radius of curvature which is strictly correlated to the interparticles spacing (S_p). The presence of some oxides characterised by extremely reduced dimensions do not allow however an exact calculation of S_p and the Orowan strengthening for these samples.

The increase in the elongation might be also correlated to the reduced oxides size and in particular to the improved interfacial bonding of smaller inclusions [34,35]. It is well-known, in fact, that ductile fractures in metallic materials arise due to the nucleation and growth of cavities. The formation of these cavities is strictly correlated to the presence of second phases [36]. The voids can indeed nucleate as a consequence of particle-matrix debonding, if the local stress exceeds the interfacial bonding, or as particle cracking, if the stress exceeds particle strength. [37]. The debonding mechanism for the L-DED 316L samples is demonstrated by the presence of spherical particles in the dimples of the fracture surface (Figure 11). When the fracture arises based on this mechanism, a higher elongation will be observed as the inclusions size decreases thanks to the enhanced interfacial bonding [36].

These interesting mechanical properties of L-DED 316L samples built using N_2 SG or BC can be also due to the N pick-up that arises during the L-DED process. The slightly higher N content of BC samples can also be the

reason for the its higher mechanical properties. As previously described, in fact, nitrogen has a strong solution strengthening effect on 316L by maintaining the same ductility [25].

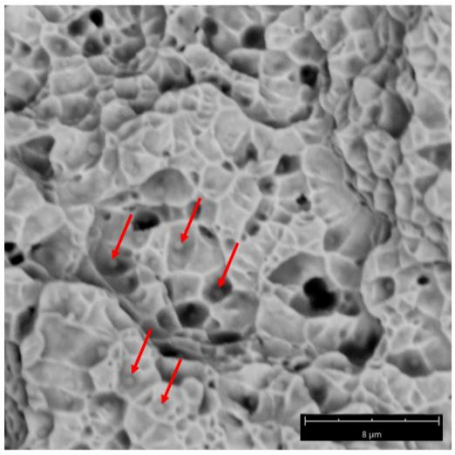

Figure 11 Fracture surface of SG 316L sample of SG samples

In Table 2, the comparison of the mechanical data with literature shows that the present results are in line with the tensile properties of L-DED 316L samples built using similar processing conditions. The tensile properties of 316L samples built with recycled powder in the same SG conditions as those of the present work are reported [16]. These samples were characterised by a larger amount of oxides and it can be noticed that the elongation is strongly affected by the inclusion content as the higher is the oxide content the lower is ε. Among these samples, the BC ones were characterised by the highest YS and UTS probably due to the combined effect of the reduced oxide size and the higher N content.

Data obtained by different authors in similar conditions are also reported [11,12]. However it is hard to correctly compare the tensile data only based on the different environmental conditions because, as previously stated, they can be affected by a considerable amount of factors such as process parameters, powder composition and oxide content.

The tensile properties of wrought 316L are also reported for comparison and it is evident that with L-DED it is possible to achieve markedly higher YS but lower elongation. The high YS values recorded for L-DED samples are mainly due to the refinement of the microstructure obtained thanks to the rapid cooling. The UTS values of L-DED samples are only slightly higher than the wrought ones, probably because of the lower level of work hardening of AM samples [38].

Table 2 Mechanical properties of 316L L-DED samples processed in different conditions and compared with literature data

Conditions	YS (MPa)	UTS (MPa)	ε (%)	Ref.
316L L-DED N_2 SG	469±3	628±7	31±2	Current work
316L L-DED N_2 BC	530±5	670±6	34±1	Current work
316L L-DED N_2 SG used powders	458 ± 30	652 ± 44	16 ± 2	[16]
316L L-DED horizontal BC	576.0	776.0	33.0	[11]
316L L-DED Ar SG	558.0	639.0	21.0	[12]
316L Wrought	220-270	520-560	40-45	[39]

4. Conclusions

The effect of the L-DED processing conditions on the quality of 316L parts was investigated, and the main results are summarised as follows:

- The oxide content and dimensions are influenced by the building conditions. The samples produced in a build chamber are characterised by the presence of finer oxides. On the other hand, LECO analyses confirmed that oxide content is doubled when using only the shielding gas.
- The samples microstructure, in terms of cellular dendrite size, phase composition and cell size, is not strongly affected by the processing atmosphere. Only slight differences as regards the dendrite size were observed.
- The mechanical properties are affected by the presence of a N_2-filled build chamber. The most protective condition of build chamber allows an increase in the yield strength and elongation values, which was therefore mainly attributed to the different size of the Mn-Si oxide particles and to the different N content.

To conclude, this study showed that mechanical properties of L-DED 316L samples built with shielding gas or N_2-filled build chamber are extremely high with respect to those of the conventionally processed ones. The yielding strength of 316L is in fact about doubled as a consequence of the AM processing. The comparison of the protective conditions showed that the shielding gas was slightly less effective than that of the N_2-filled build chamber one in limiting the material oxidation.

Funding: This work was supported by Prima Industrie SpA

References

[1] D. Kianersi, A. Mostafaei, A.A. Amadeh, Resistance spot welding joints of AISI 316L austenitic stainless steel sheets: Phase transformations, mechanical properties and microstructure characterizations, Mater. Des. 61 (2014) 251–263. doi:10.1016/j.matdes.2014.04.075.

[2] M. Ma, Z. Wang, X. Zeng, A comparison on metallurgical behaviors of 316L stainless steel by selective laser melting and laser cladding deposition, Mater. Sci. Eng. A. 685 (2017) 265–273. doi:10.1016/j.msea.2016.12.112.

[3] M. Dadfar, M.H. Fathi, F. Karimzadeh, M.R. Dadfar, A. Saatchi, Effect of TIG welding on corrosion behavior of 316L stainless steel, Mater. Lett. 61 (2007) 2343–2346. doi:https://doi.org/10.1016/j.matlet.2006.09.008.

[4] W.E. Frazier, Metal additive manufacturing: A review, J. Mater. Eng. Perform. 23 (2014) 1917–1928. doi:10.1007/s11665-014-0958-z.

[5] S.M. Thompson, L. Bian, N. Shamsaei, A. Yadollahi, An overview of Direct Laser Deposition for additive manufacturing; Part I: Transport phenomena, modeling and diagnostics, Addit. Manuf. 8 (2015) 36–62. doi:10.1016/j.addma.2015.07.001.

[6] M. Javidani, J. Arreguin-Zavala, J. Danovitch, Y. Tian, M. Brochu, Additive Manufacturing of AlSi10Mg Alloy Using Direct Energy Deposition: Microstructure and Hardness Characterization, J. Therm. Spray Technol. 26 (2017) 587–597. doi:10.1007/s11666-016-0495-4.

[7] A. Yadollahi, N. Shamsaei, S.M. Thompson, D.W. Seely, Effects of process time interval and heat treatment on the mechanical and microstructural properties of direct laser deposited 316L stainless steel, Mater. Sci. Eng. A. 644 (2015) 171–183. doi:10.1016/j.msea.2015.07.056.

[8] G. Marchese, X. Garmendia Colera, F. Calignano, M. Lorusso, S. Biamino, P. Minetola, D. Manfredi, Characterization and Comparison of Inconel 625 Processed by Selective Laser

Melting and Laser Metal Deposition , Adv. Eng. Mater. (2016) 1–9. doi:10.1002/adem.201600635.
[9] B.E. Carroll, T.A. Palmer, A.M. Beese, Anisotropic tensile behavior of Ti-6Al-4V components fabricated with directed energy deposition additive manufacturing, Acta Mater. 87 (2015) 309–320. doi:10.1016/j.actamat.2014.12.054.
[10] K. Saeidi, X. Gao, Y. Zhong, Z.J. Shen, Hardened austenite steel with columnar sub-grain structure formed by laser melting, Mater. Sci. Eng. A 625 221–229 Contents. 625 (2015) 221–229.
[11] M. Ziętala, T. Durejko, M. Polański, I. Kunce, T. Płociński, W. Zieliński, M. Łazińska, W. Stępniowski, T. Czujko, K.J. Kurzydłowski, Z. Bojar, The microstructure, mechanical properties and corrosion resistance of 316L stainless steel fabricated using laser engineered net shaping, Mater. Sci. Eng. A. 677 (2016) 1–10. doi:10.1016/j.msea.2016.09.028.
[12] K. Zhang, S. Wang, W. Liu, X. Shang, Characterization of stainless steel parts by Laser Metal Deposition Shaping, J. Mater. 55 (2014) 104–119. doi:10.1016/j.matdes.2013.09.006.
[13] A. Saboori, G. Piscopo, M. Lai, A. Salmi, S. Biamino, G. Piscopo, M. Lai, A. Salmi, S. Biamino, Journal Pre-proof, (2020).
[14] F. Mazzucato, A. Aversa, R. Doglione, S. Biamino, A. Valente, M. Lombardi, Influence of Process Parameters and Deposition Strategy on Laser Metal Deposition of 316L Powder, (2019) 11–14.
[15] M. Ma, Z. Wang, D. Wang, X. Zeng, Control of shape and performance for direct laser fabrication of precision large-scale metal parts with 316L Stainless Steel, Opt. Laser Technol. 45 (2013) 209–216.
[16] A. Saboori, A. Aversa, F. Bosio, E. Bassini, E. Librera, M. De Chirico, S. Biamino, D. Ugues, P. Fino, M. Lombardi, An investigation on the effect of powder recycling on the microstructure and mechanical properties of AISI 316L produced by Directed Energy Deposition, Mater. Sci. Eng. A. 766 (2019). doi:https://doi.org/10.1016/j.msea.2019.138360.
[17] D. Eo, S. Park, J. Cho, Inclusion evolution in additive manufactured 316L stainless steel by laser metal deposition process, Mater. Des. J. 155 (2018) 212–219.
[18] M. Song, X. Lin, F. Liu, H. Yang, W. Huang, Effect of environmental oxygen content on the oxide inclusion in laser solid formed AISI 420 stainless steel, Mater. Des. 90 (2016) 459–467. doi:10.1016/j.matdes.2015.11.003.
[19] K. Saeidi, X. Gao, F. Lofaj, L. Kvetková, Z.J. Shen, Transformation of austenite to duplex austenite-ferrite assembly in annealed stainless steel 316L consolidated by laser melting, 633 (2015) 463–469.
[20] X. Lou, P.L. Andresen, R.B. Rebak, Oxide inclusions in laser additive manufactured stainless steel and their effects on impact toughness and stress corrosion cracking behavior, J. Nucl. Mater. (2018) 182–190. doi:10.1016/j.jnucmat.2017.11.036.
[21] F. Bosio, A. Saboori, A. Lacagnina, E. Librera, M. De Chirico, S. Biamino, P. Fino, M. Lombardi, Directed Energy Deposition of 316L Steel: Effect of Type of Powders and Gas Related Parameters, Proc. EURO PM2018. (2018) 1–6.
[22] F. Yan, W. Xiong, E. Faierson, G.B. Olson, Characterization of nano-scale oxides in austenitic stainless steel processed by powder bed fusion, 155 (2018) 104–108.
[23] K. Geenen, A. Röttger, W. Theisen, Corrosion behavior of 316L austenitic steel processed by selective laser melting, hot-isostatic pressing, and casting, Mater. Corros. 68 (2017) 764–775. doi:10.1002/maco.201609210.
[24] V.G. Gavriljuk, B.D. Shanina, H. Berns, Ab initio development of a high-strength corrosion-resistant austenitic steel, Acta Mater. 56 (2008) 5071–5082. doi:10.1016/j.actamat.2008.06.021.

[25] J. Boes, A. Röttger, L. Becker, W. Theisen, Processing of gas-nitrided AISI 316L steel powder by laser powder bed fusion – Microstructure and properties, Addit. Manuf. 30 (2019). doi:10.1016/j.addma.2019.100836.
[26] Z. Wang, T.A. Palmer, A.M. Beese, Effect of processing parameters on microstructure and tensile properties of austenitic stainless steel 304L made by directed energy deposition additive manufacturing, Acta Mater. 110 (2016) 226–235.
[27] M.L. Huber, A.H. Harvey, Thermal Conductivity of Gases, CRC Handb. Chem. Phys. 94th editi (n.d.) 240–241.
[28] Z. Sun, X. Tan, S. Tor, W.Y. Yeong, Selective laser melting of stainless steel 316L with low porosity and high build rates, Mater. Des. 104 (2016) 197–204.
[29] P. Guo, B. Zou, C. Huang, H. Gao, Study on microstructure , mechanical properties and machinability of efficiently additive manufactured AISI 316L stainless steel by high-power direct laser deposition, J. Mater. Process. Technol. 240 (2017) 12–22.
[30] K. Li, D. Li, D. Liu, G. Pei, L. Sun, Microstructure evolution and mechanical properties of multiple-layer laser cladding coating of 308L stainless steel, Appl. Surf. Sci. 340 (2015) 143–150. doi:10.1016/j.apsusc.2015.02.171.
[31] N. Jakse, A. Pasturel, Liquid Aluminum: atomic diffusion and viscosity from ab initio molecular dynamics., Sci. Rep. 3 (2013) 3135. doi:10.1038/srep03135.
[32] E.A. Jägle, Z. Sheng, L. Wu, L. Lu, J. Risse, A. Weisheit, D. Raabe, Precipitation Reactions in Age-Hardenable Alloys During Laser Additive Manufacturing, JOM. 68 (2016) 943–949. doi:10.1007/s11837-015-1764-2.
[33] A. Saboori, E. Padovano, M. Pavese, C. Badini, Novel Magnesium Elektron21-AlN Nanocomposites, Materials (Basel). 11 (2018). doi:10.3390/ma11010027.
[34] Nikhilesh Chawla Krishan K. Chawla, Metal matrix composites, 2013. doi:10.1007/978-1-4614-9548-2.
[35] R. Harichandran, N. Selvakumar, Effect of nano/micro B4C particles on the mechanical properties of aluminium metal matrix composites fabricated by ultrasonic cavitation-assisted solidification process, Arch. Civ. Mech. Eng. 16 (2016) 147–158. doi:10.1016/j.acme.2015.07.001.
[36] J.C. Anderson, K.D. Leaver, R.D. Rawlings, J.M. Alexander, Materials Science, n.d.
[37] P. Mummery, B. Derby, The influence of microstructure on the fracture behaviour of particulate metal matrix composites, Mater. Sci. Eng. A. 135 (1991) 221–224. doi:10.1016/0921-5093(91)90566-6.
[38] J. Suryawanshi, K.G. Prashanth, U. Ramamurty, Mechanical behavior of selective laser melted 316L stainless steel, Mater. Sci. Eng. A. 696 (2017) 113–121. doi:10.1016/j.msea.2017.04.058.
[39] I. Tolosa, F. Garciandía, F. Zubiri, F. Zapirain, A. Esnaola, Study of mechanical properties of AISI 316 stainless steel processed by “selective laser melting”, following different manufacturing strategies, Int. J. Adv. Manuf. Technol. 51 (2010) 639–647. doi:10.1007/s00170-010-2631-5.

Figure

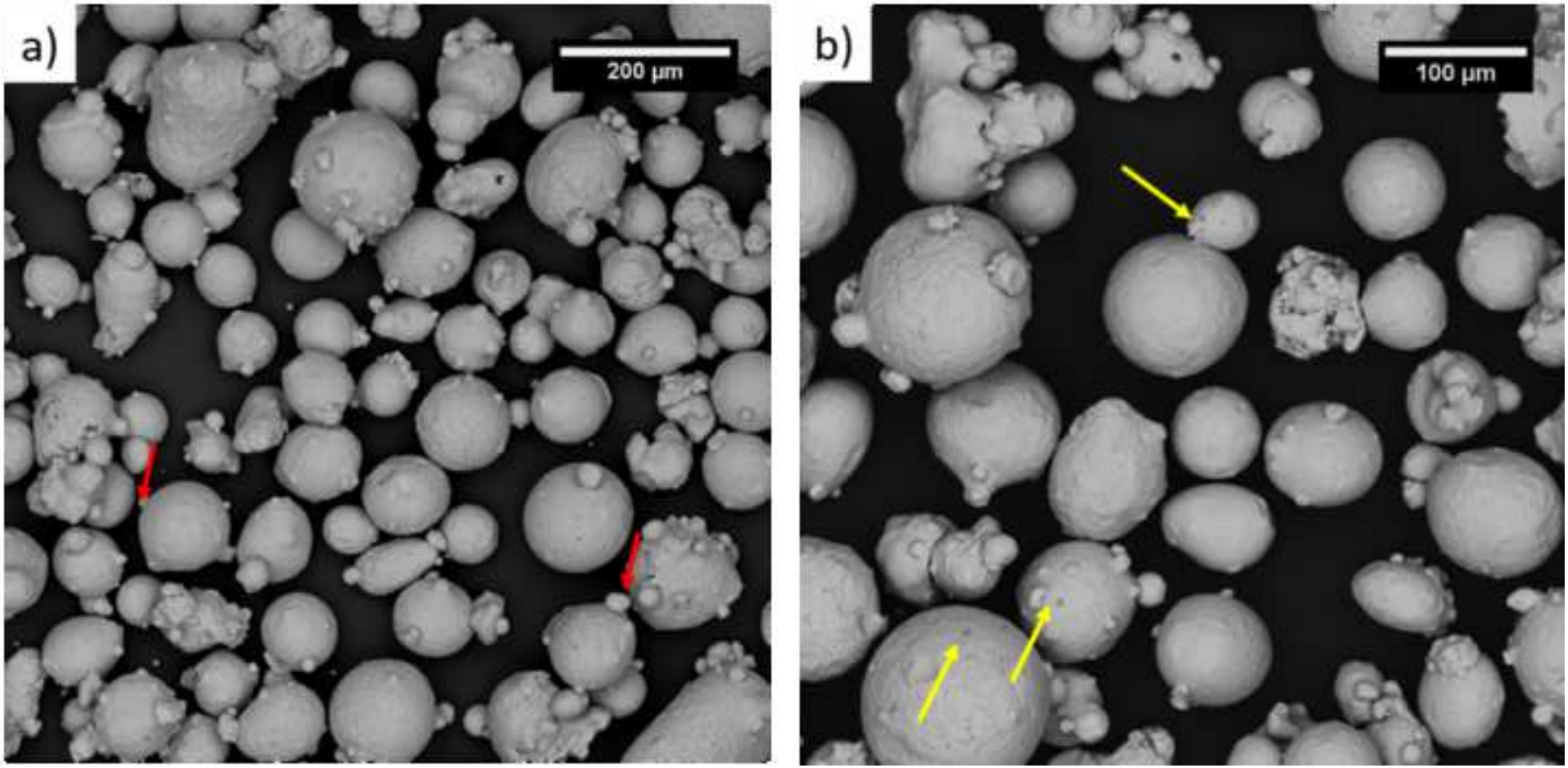

Figure

Click here to access/download;Figure;Fig. 2__.png

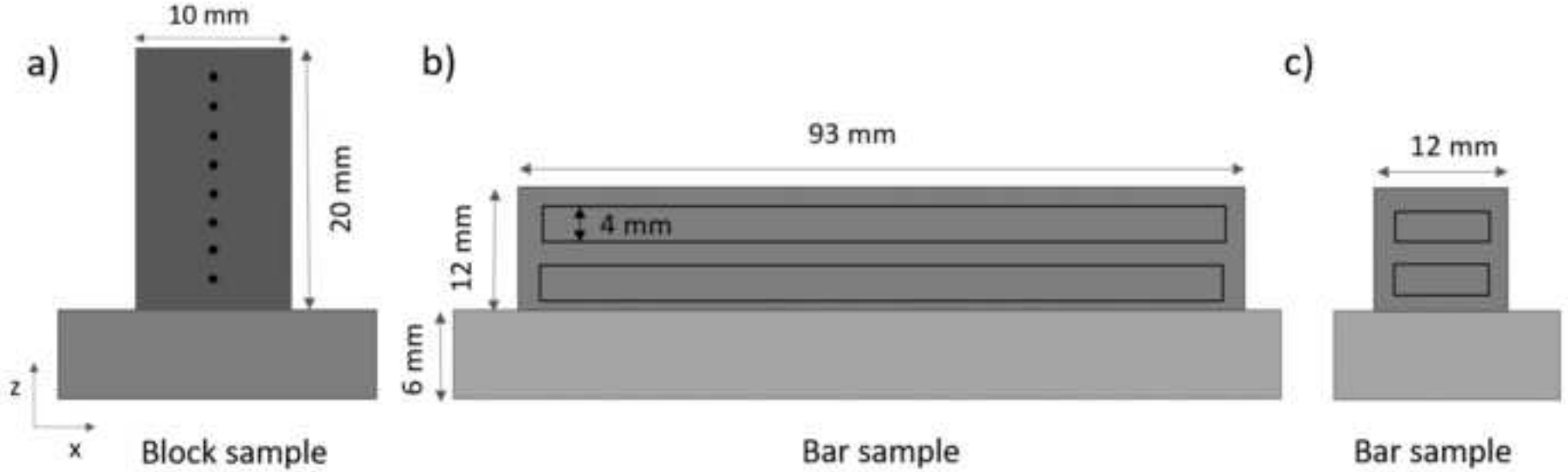

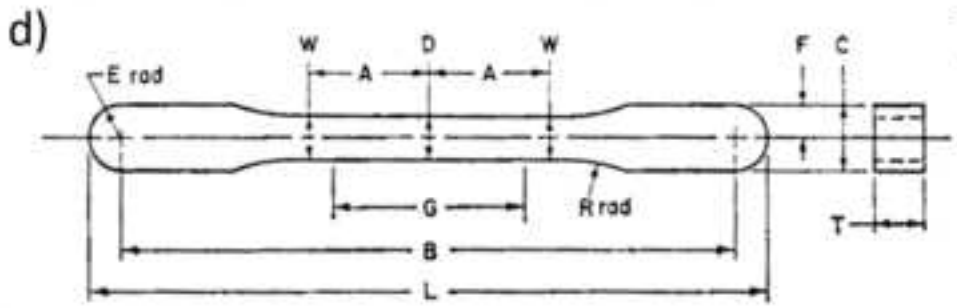

	mm		mm
G	25,4	A	15,9
D	5,7	B	80,9
W	5,9	L	89,6
T	4,0	C	8,7
R	25,4	F=E	4,3

Figure

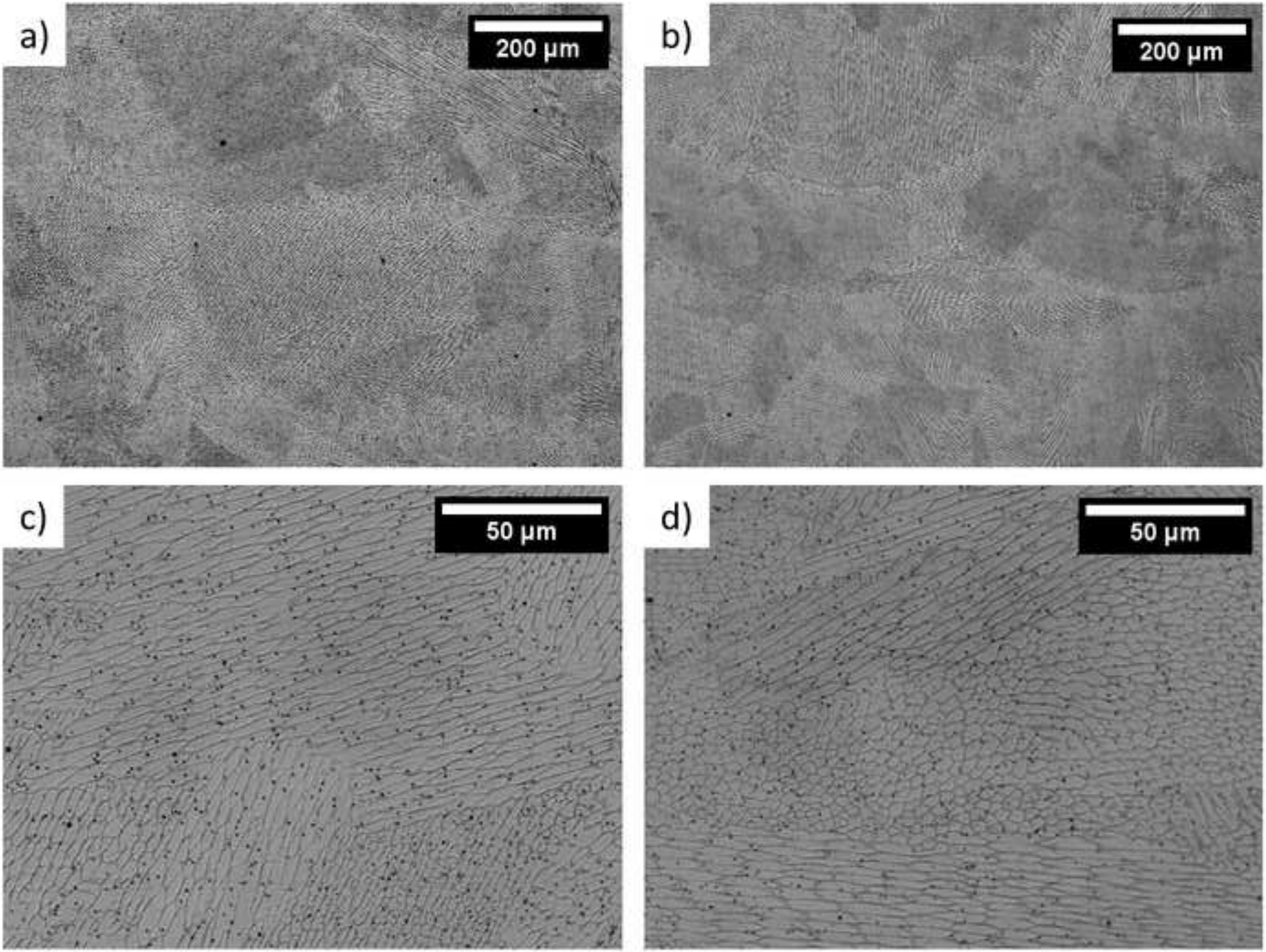

Figure

Click here to access/download;Figure;Fig. 4__.png

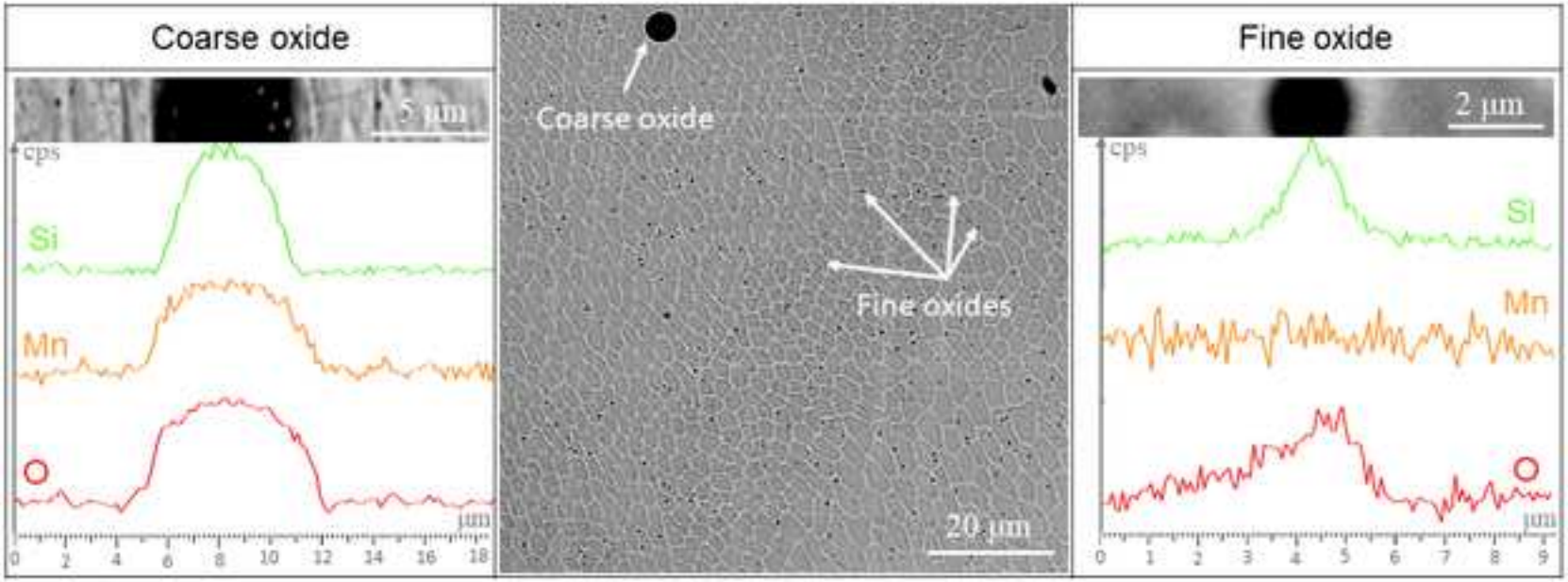

Figure

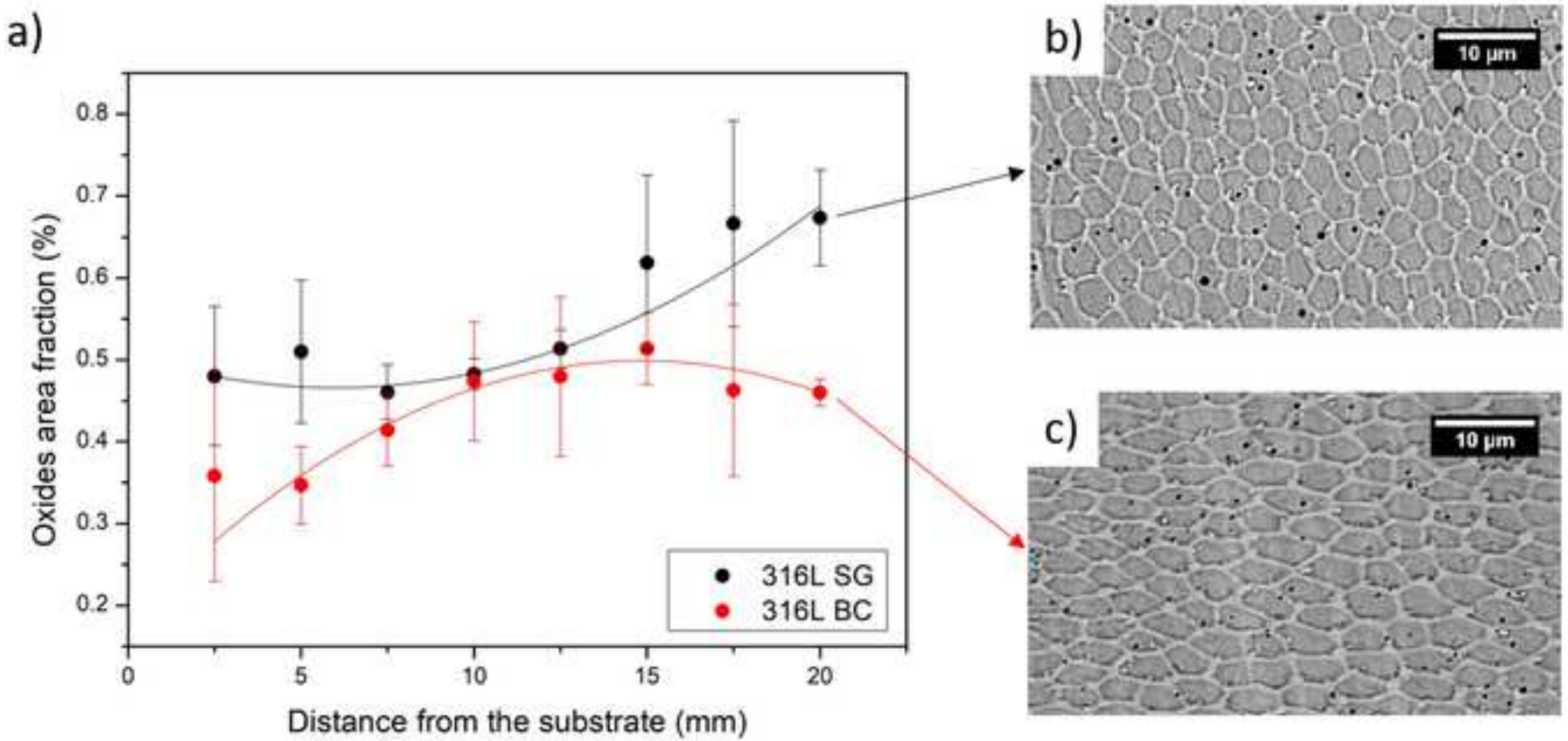

Figure

Click here to access/download;Figure;Fig 6_.png

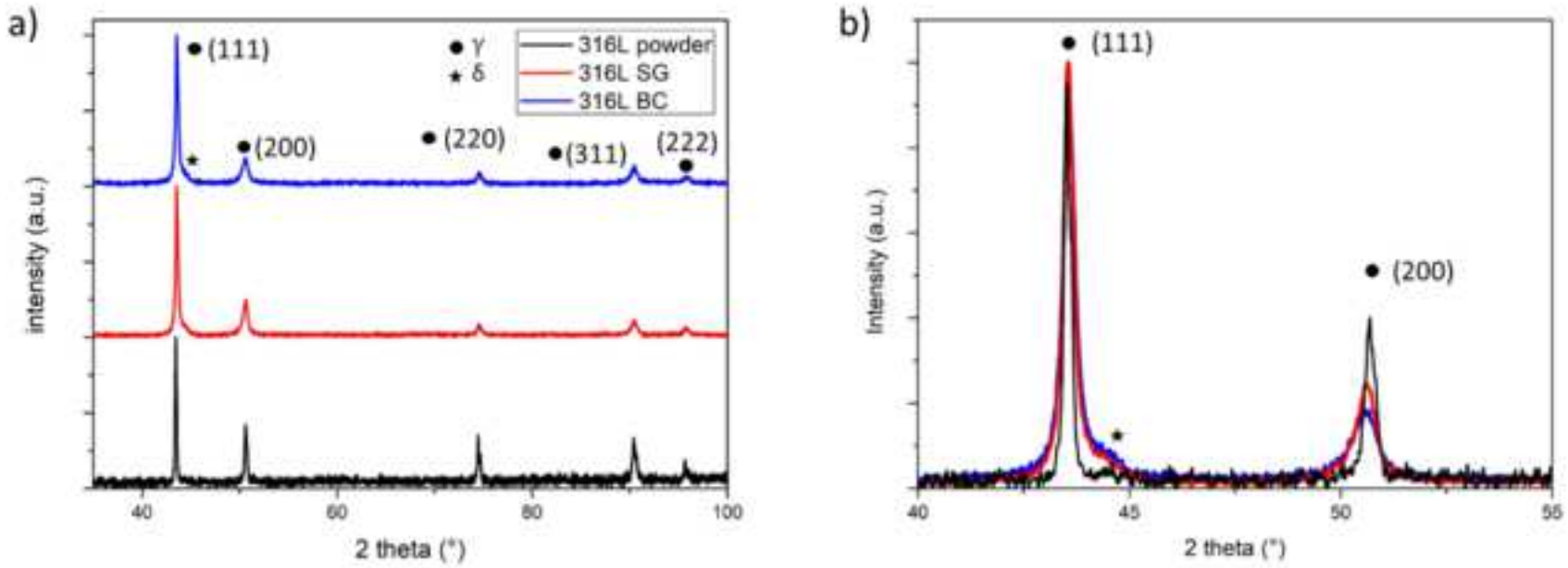

Figure

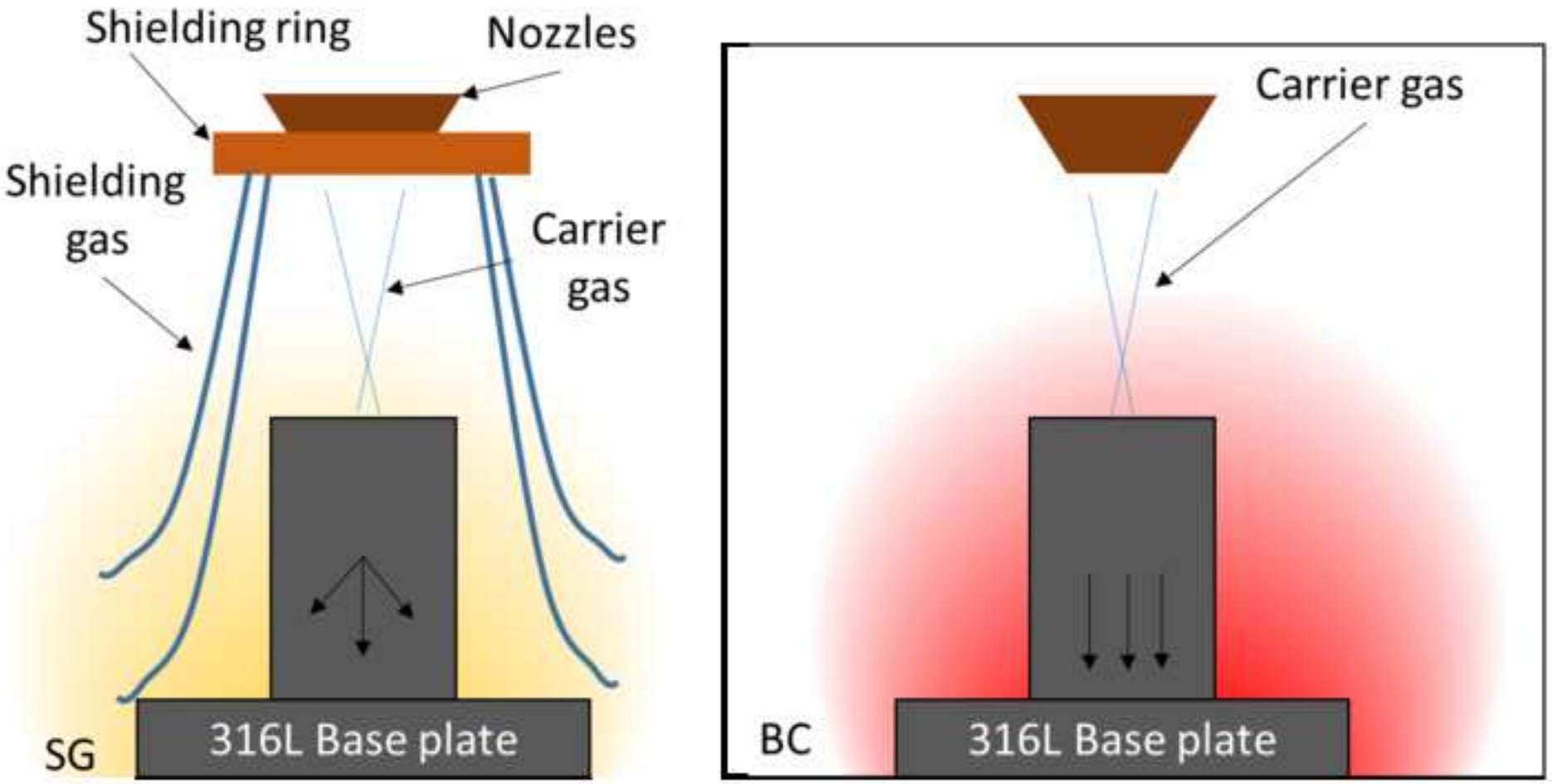

Figure

Click here to access/download;Figure;Fig 8_.png

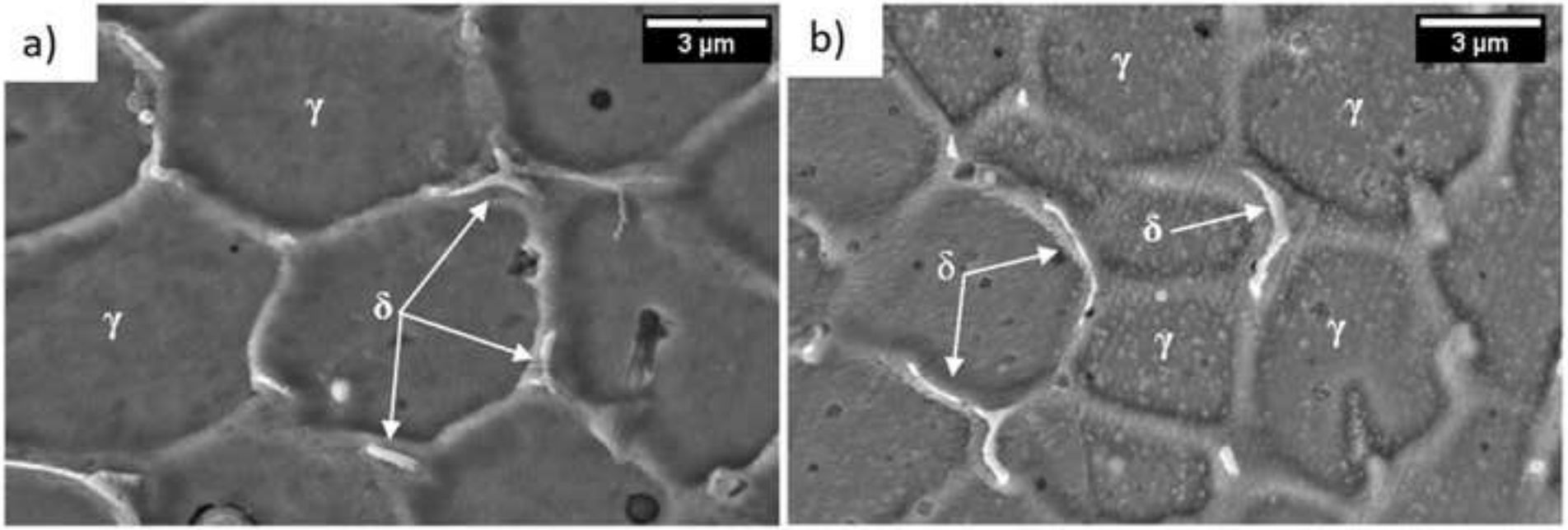

Figure

Click here to access/download;Figure;Fig 9_.png

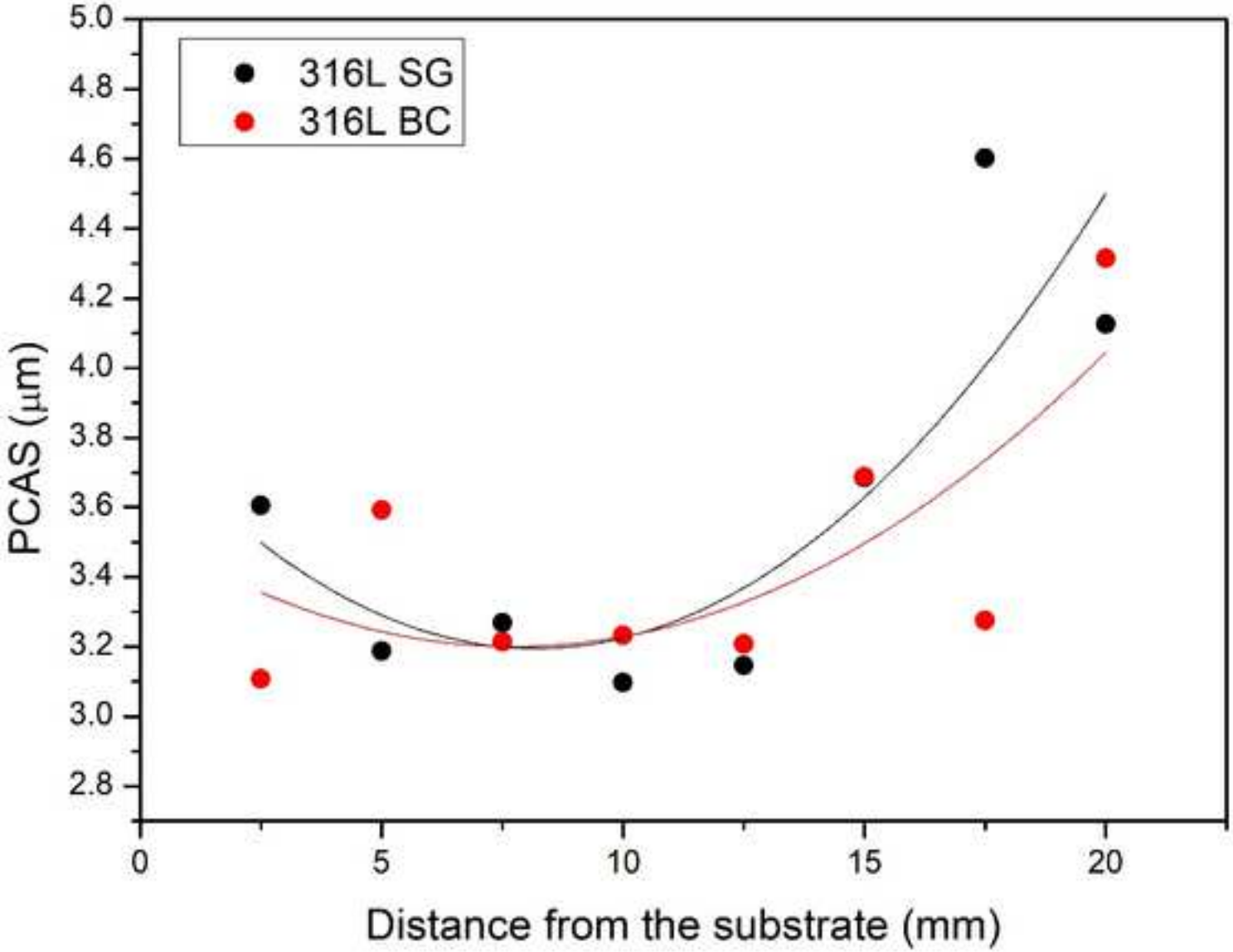

Figure

Click here to access/download;Figure;Fig 10_.png

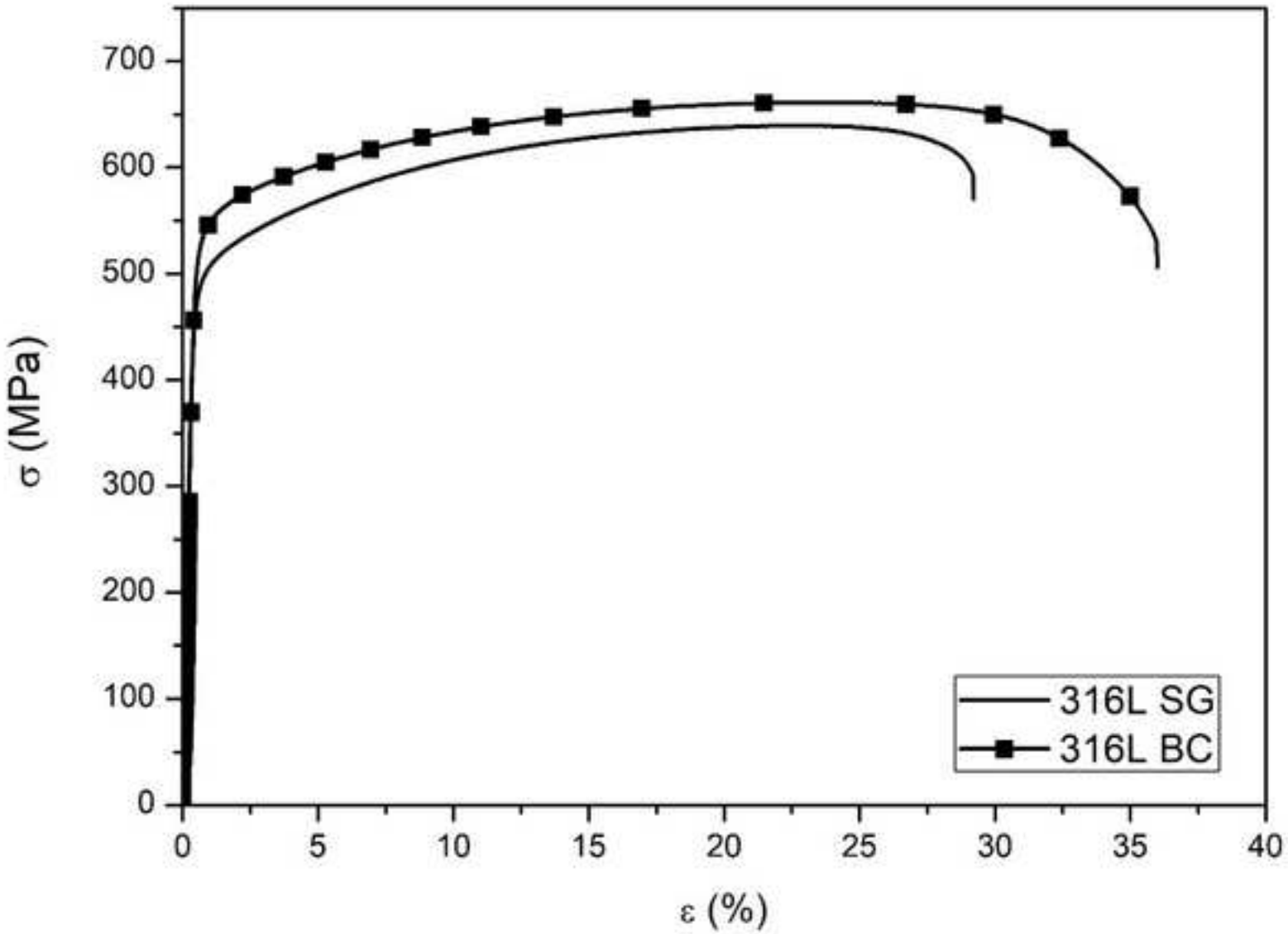

Figure

Click here to access/download;Figure;Fig 11_.png

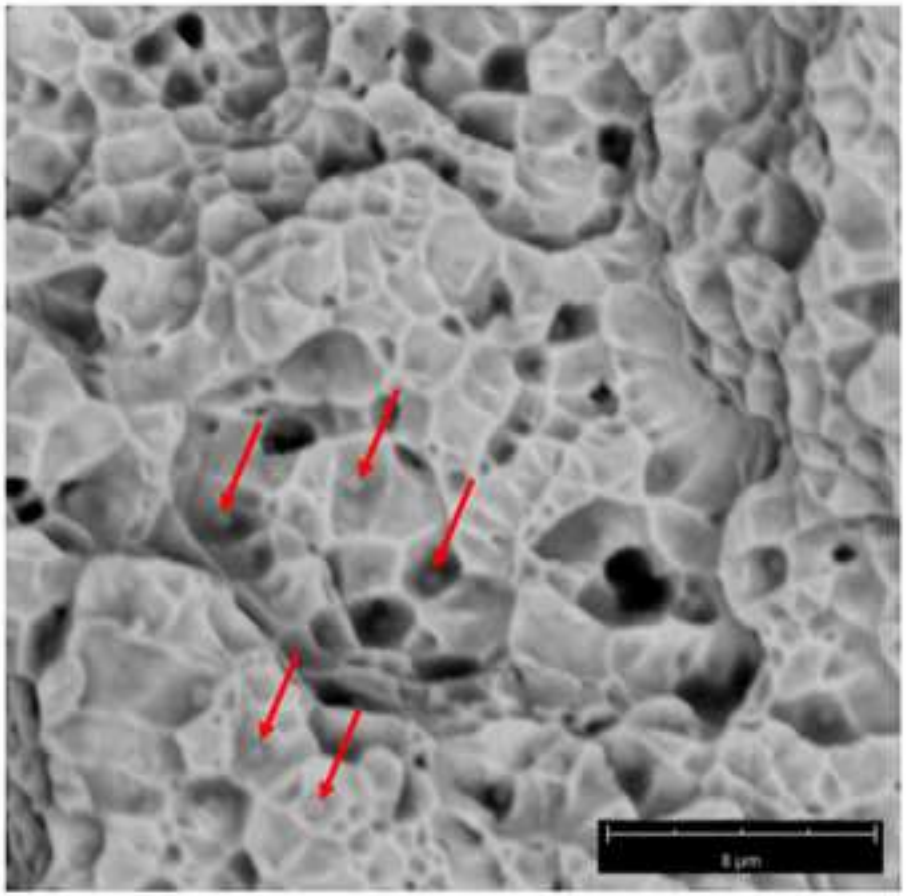

Table

Table

Declaration of interests

☒ The authors declare that they have no known competing financial interests or personal relationships that could have appeared to influence the work reported in this paper.

☐The authors declare the following financial interests/personal relationships which may be considered as potential competing interests:

Author Statement

Methodology Alberta Aversa Abdollah Saboori Erica Librera and Michele de Chirico

Conceptualization Michele de Chirico, Mariangela Lombardi and Sara Biamino

Software and investigations Erica Librera, Abdollah Saboori and Alberta Aversa

Writing - Original Draf Alberta Aversa and Abdollah Saboori

Writing - Review & Editing Mariangela Lombardi, Sara Biamino and Paolo Fino

Supervision Paolo Fino